# 8.91% Power Conversion Efficiency for Polymer Tandem Solar Cells

*Abd. Rashid bin Mohd Yusoff, Seung Joo Lee, Hyeong Pil Kim, Fabio Kurt Shneider, Wilson Jose da Silva, and Jin Jang**

**A power conversion efficiency of up to 8.91% is obtained for a solution-processed polymer tandem solar cells based on a large-bandgap polymer, poly(4,4-dioctyldithieno(3,2-b:2′,3′-d)silole)-2,6-diyl-*alt*-(2,1,3-benzothiadiazole)-4,7-diyl) with a polymeric interconnecting layer to electrically connect the front and rear subcells, demonstrating that proper device and interface engineering are can improve the performance of polymer tandem solar cells.**

## 1. Introduction

Polymer solar cells have seen a rapid improvement in efficiency, especially in single-junction cells. The best reported single-junction efficiency is 9.2%[1] according to H. Wu in 2012. These authors proposed a promising donating polymer, thieno[3,4-*b*]thiophene/benzodithiophene (PTB7), and hole transporting material, poly[9,9-bis(3′-(*N,N*-dimethylamino) propyl)-2,7-fluorene]-alt-2,7-(9,9-dioctylfluorene)] (PFN), that demonstrate a high short-circuit current density ($J_{sc}$) and fill factor (FF).

Despite these advances, there are two unavoidable major losses in most single-junction cells. These losses are i) the thermalization of excitations, and ii) the transmission of photons. The first loss takes place when photons (at wavelengths <700 nm) with higher energy than the energy bandgap of the polymer or organic semiconductor are absorbed. This corresponds to a common loss in solar-cell conversion and the development of such an ultrafast platform, possibly operating at high temperature, which is able to provide a better use of up to 40% of the free energy in the photons of the entire visible spectrum. The latter is due to the transmission of photons, having relatively lower energy than the bandgap energy, through the cell without being absorbed. In this case, the thickness of the absorbing material should be equal to the absorption length of the photon of energy equal to bandgap energy.

Hence, to overcome the aforementioned losses, a new device architecture, the tandem solar cell, was proposed by Hiramoto and his co-workers.[2] In their work, they established an ultra-thin Au interstitial layer as conductive interconnecting layer (ICL), where the photovoltage was almost doubled. Additionally, they found that the photocurrent density depends on the Au layer thickness. The absence of this conductive ICL would form a barrier, and the charge build up at the interface would significantly affect the device's performance at the interface. Thus, to avoid excess of one particular charge carrier at the ICL, it is imperative that the photocurrent density of each subcell is balanced. It is worth mentioning that both conductivity of the ICL and current matching of the front and rear subcells are very important in tandem solar cells. Although this current matching issue is usually performed by having the suitable active layer thicknesses, it can never resolve the problem caused by the inferior conductivity of an ICL. There are other important issues come into account in desiging high-performance tandem solar cells, such as the selection of active materials for the front and rear subcells, the morphology of each deposited layer, and the robustness of the ICL.

Since then, ICLs including doped p–n organic heterojunctions,[3,4] thin metal layers,[5–9] and metal oxides,[7,9–11] have increasingly been applied to electrically connect the two subcells. In tandem cells, the ICL serves as the charge recombination zone between the front and rear subcells; the ICL is vital in realizing high performance in tandem cells.

The tandem concept is appealing because i) most organic semiconductor materials have relatively strong absorption efficients $\geq 10^5$ $cm^{-1}$, which can balance low mobility and high absorption in even <100 nm thin devices, and ii) the thickness of light-absorbing layers is limited by a relatively low charge-carrier mobility and small exciton diffusion length.[12] Hence, high photocurrents are possible in tandem cells because of the high complementary of the absoption spectra in the photoactive layers.

Furthermore, efficiency is enhanced by the summation of photovoltages or photocurrents, because tandem cells are connection either in series or parallel. Thus, fewer conditions are established on the sheet resistance of the transparent electrode, allowing for large-area solar-cell structures and/or less conductive electrodes.[13–15]

Prof. A. R. b. M. Yusoff, S. J. Lee,
H. P. Kim, Prof. J. Jang
Department of Information Display
Advanced Display Research Center
Kyung Hee University
Dongdaemoon-gu, 130–701, Seoul, South Korea
E-mail: jjang@khu.ac.kr
F. K. Shneider, Dr. W. J. da Silva
Universidade Tecnologica Federal do Parana
GPGEI – Av. Sete de Setembro, 3165 – CEP, 80230–901,
Curitiba, Parana, Brazil

DOI: 10.1002/adfm.201303471

Although the efficiency in a single-junction solar cell is approaching double digits,[16–18] significant improvements, especially on device stability, need to be made before mass production can be realized. There are a few methods to enhance the stability, such as: a) minimal use of reactive metals, b) employment of air-stable materials including transition metal oxides, c) use of air-stable active materials, d) encapsulation, and e) utilization of inverted structures. Inverted structures avoid ITO/PEDOT:PSS interfaces, which weaken device stability.

The first fabricated inverted tandem solar cell was published by Sun and co-workers,[19,20] who used poly(3-hexylthiophene):[6,6]-phenyl-$C_{61}$-butyric acid methyl ester (P3HT:$PC_{60}$BM) BHJ solar cells in both front and rear subcells. In their tandem cell, a complicated stack of thermally evaporated $MoO_3$ and ultrathin multiple metal layers of Ag, Al, and Ca was used as their ICL. Although the deposition of this ICL is relatively complicated, they were able to obtain an ideal summation of the open-circuit voltage ($V_{oc}$) of the front and rear subcells, which leads 2.8% PCE. Thereafter, the efficiency of the tandem cell was further improved to 5.1% by Yang and co-workers. They employed a large bandgap P3HT:$PC_{60}$BM and a low bandgap poly(4,4-dioctyldithieno(3,2-b:2′,3′-d)silole)-2,6-diyl-*alt*-(2,1,3-benzothiadiazole)-4,7-diyl):[6,6]phenyl-$C_{71}$-butyric acid methyl ester (PSBTBT:$PC_{70}$BM) for the front and rear subcells, respectively.[21] In their study, thermally evaporated $MoO_3$, Al and solution processed ZnO solution were used as ICL. Later, the new concept and the first all solution processed ICL (PEDOT:PSS/ZnO) have been put forward by Jen and co-workers,[22] where the authors achieved a PCE of 2.9%. More recently, Yusoff and co-workers reported another fully solution-processed inverted polymer tandem solar cell with a poly[(4,4′-bis(3-ethyl-hexyl)dithieno[3,2-b:″3′-d]silole)-2,6-diyl-alt-(2,5-(3-(2-ethyl-hexyl)thiophen-2-yl)thiazolo[5,4-d]thiazole]: indene-$C_{60}$ bisadduct (PSEHTT:$IC_{60}$BA) and PSBTBT:$PC_{70}$BM as front and rear subcells, respectively.[23] The ICL consists of titanium oxide ($TiO_2$)/graphene oxide (GO) and yields PCE of 8.40% without any loss in the summation of $V_{oc}$s of the tandem cell. Though the $TiO_2$ is a promising interlayer material for tandem cells, the $TiO_2$ layer formation requires hydrolysis, which might affect the throughput of the tandem cell production and storage stability of the $TiO_2$ solution.

## 2. Results and Discussion

In this study, we provide an efficient solution for the processed inverted tandem polymer solar cell (**Figure 1**a), combining a large bandgap semiconducting polymer (PSEHTT, Figure 1a) and a low bandgap polymer (PSBTBT, Figure 1a). We assert that a single*junction solar cell comprising an active layer of PSEHTT blended with $IC_{60}$BA provides an efficient single junction of 5.99%. Moreover, the rear subcell of PSBTBT with $PC_{70}$BM provides a maximum single-junction PCE of 4.99%. PSEHTT:$IC_{60}$BA front subcell gives a high $V_{oc}$ = 0.91 V in the inverted configuration. The low-bandgap rear subcell with PSBTBT:$PC_{70}$BM is moderate ($V_{oc}$ = 0.64 V). With bandgaps of 1.8 and 1.5 eV, respectively, the optical absorption of these two photoactive layers is complementary and covers a wide range of spectral responses. We demonstrate that the inverted tandem cell provides a PCE of 8.91%, with 5.99% and 4.99% in the front and rear subcells, respectively. Figure 1b,c demonstrate a schematic diagram of the fully processed tandem solar cell (except bottom and top electrodes) and the proposed energy-level diagram. The excitons are photoexcited in the front and rear subcells. PSEHTT:$IC_{60}$BA and PSBTBT:$PC_{70}$BM photoactive layers and electrons are injected into the PEIE cathode and holes of the $MoO_3$ anode. The front and rear subcells are electrically connected with a PEDOT:PSS/PEIE ICL that accepts holes from the front cell, electrons from the rear cell, and subsequently recombines them. The tandem solar cell architecture prohibits individual testing of its subcells. Thus, we constructed corresponding single-junction solar cells as reference cells with photoactive layers from the same synthesis batch fabricated under identical film-deposition conditions.

Electron and hole transport layers (E/HTL) greatly influence the inverted single-junction solar cell. It is imperative to optimize the thicknesses of ETL and HTL to prevent exciton quenching and loosing of charge at the anode side, as well as the thickness of the photoactive layers. Firstly, to evaluate performance in tandem cells, a series of single-junction solar cells with different bulk heterojunction (BHJ) layer thicknesses were prepared using the optimized processing conditions and the devices were characterized in detail.

From **Figure 2**a, the mean spectral average internal quantum efficiency (IQE) is 70% for PSEHTT:$IC_{60}$BA with a standard deviation of 2%. Next, we evaluated photovoltaic performance of single-junction PSEHTT:$IC_{60}$BA BHJ solar cells in relation to the PSEHTT:$IC_{60}$BA BHJ thickness. As anticipated in the inverted device architecture, device performance directly depends on the photoactive layer thicknesses (ITO/PEIE/PSEHTT:$IC_{60}$BA/HTLs/LiF:Al). In these evaluation experiments, PEIE served as the ETL.

Figure 2b shows the J–V characteristics of the single junction with various thicknesses ranging from 100 nm to 130 nm under 100 mW/$cm^2$AM1.5G illumination. Regardless of the thickness of the PSEHTT:$IC_{60}$BA BHJ layer, the $V_{oc}$s of all cells are 0.91 V (**Table 1**). As predicted, this occurred because $V_{oc}$ depends mostly on the energy levels of the photoactive layer. Conversely to $V_{oc}$, the $J_{sc}$ of the cell changes drastically with the thickness of PSEHTT:$IC_{60}$BA BHJ layer. The $J_{sc}$ shows oscillatory behavior because $J_{sc}$ depends on the number of photons absorbed into the PSEHTT:$IC_{60}$BA BHJ layer. However, the photocurrent at 130 nm is less compared to that at 120 nm. Low $J_{sc}$ in the PSEHTT:$IC_{60}$BA BHJ is attributed to the following: i) as the thickness of the PSEHTT:$IC_{60}$BA BHJ layer

**Table 1.** Device performance of PSEHTT:$IC_{60}$BA-based inverted single junction solar cells with different BHJ layer thicknesses and different HTLs.

| Active layer thickness [nm] | HTL | $J_{sc}$ [mA/$cm^2$] | $V_{oc}$ [V] | FF [%] | PCE [%] |
|---|---|---|---|---|---|
| 110 | PEDOT:PSS | 9.92 | 0.91 | 64.29 | 5.74 |
| 120 | PEDOT:PSS | 9.98 | 0.91 | 66.63 | 5.99 |
| 130 | PEDOT:PSS | 8.42 | 0.91 | 63.80 | 4.84 |
| 100 | $MoO_3$ | 9.51 | 0.91 | 64.19 | 5.49 |
| 100 | GO | 7.89 | 0.91 | 64.23 | 4.66 |

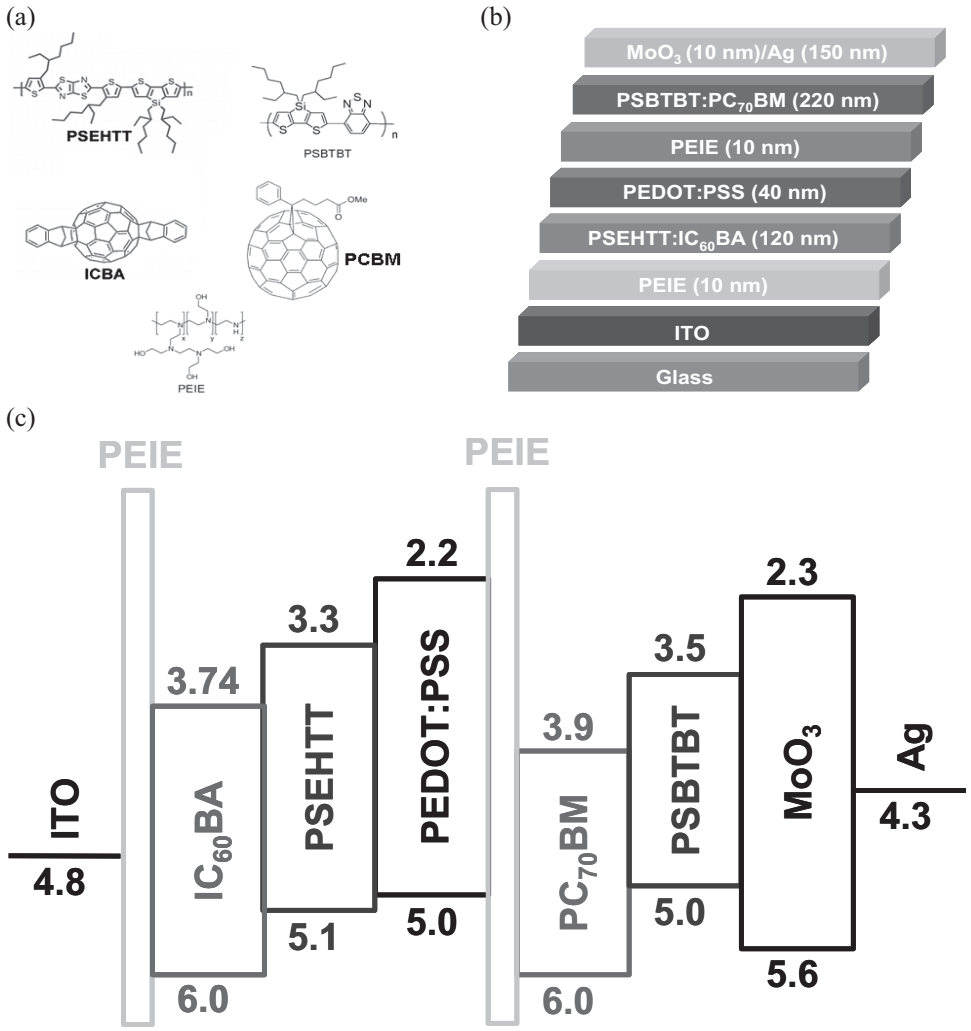


**Figure 1.** a) Chemical structures of the polymers (PSEHTT and PSBTBT), fullerene (ICBA and PCBM) as well as PEIE used in polymer tandem solar cells. b) Tandem device structures: Glass/ITO/PEIE/PSEHTT:$IC_{60}BA$/PEDOT:PSS/PEIE/PSBTBT:$PC_{70}$-BM/$MoO_3$/Ag. c) Energy-level diagram of the polymer tandem solar cells.

increases, the electric field inside the PSEHTT:$IC_{60}BA$ BHJ layer decreases at the constant bias voltage. Since the exciton dissociation rate depends on the electric field, the dissociation rate of excitons becomes smaller at lower electric fields, and ii) the decrease of $J_{sc}$ in thicker PSEHTT:$IC_{60}BA$ BHJ layers is due to an increase in recombination. A thicker cell has a longer pathway for charge collection; therefore, the probability for separated charges to recombine increases. Moreover, under the short-circuit conditions and due to lower electric fields in thicker cells, the drift of charges reduces in speed and the probability of the separated charges to recombine increases. Thus, lower $J_{sc}$ in 130 nm thick cells results from an increased recombination. Meanwhile, the fill factor (FF) decreases with the increase of the PSEHTT:$IC_{60}BA$ BHJ layer. Because the maximum power point on a J–V curve in an electric field is smaller than when at short-circuit condition, there is a lower dissociation rate and a higher recombination rate.[24] The electric field in thicker cells becomes smaller due to the longer distance between the electrodes. Therefore, recombination of charge carriers at the maximum power point is prominent in thicker devices, resulting in a low FF.

Figure 2c,d illustrate the measured external quantum efficiency (EQE) and the absorption spectra of single junction solar cells. One sees the EQE highest peak is about 62%, and the average absorption in the visible regime is around 55%. The integrated EQEs for 110, 120, and 130 nm devices are 9.51, 9.59, and 8.38 mA/cm$^2$, respectively. These values are in agreement with the obtained $J_{sc}$ values from J–V characteristics.

Secondly, an additional evaluation experiment was executed to determine the best single-junction photovoltaic performance based on PSBTBT:$PC_{70}BM$ BHJ layers. As discussed above, the same behavior can be seen and there is a strong dependency of photovoltaic performance in different photoactive layer thicknesses. In this evaluation study, our inverted device structure consisted of ITO/ETL/PSBTBT:$PC_{70}BM$/$MoO_3$/Ag, where $MoO_3$ was employed as hole transport layer.

**Figure 3**a depicts the IQE curves with various photoactive layer thicknesses (from 200 to 230 nm). The mean spectrally

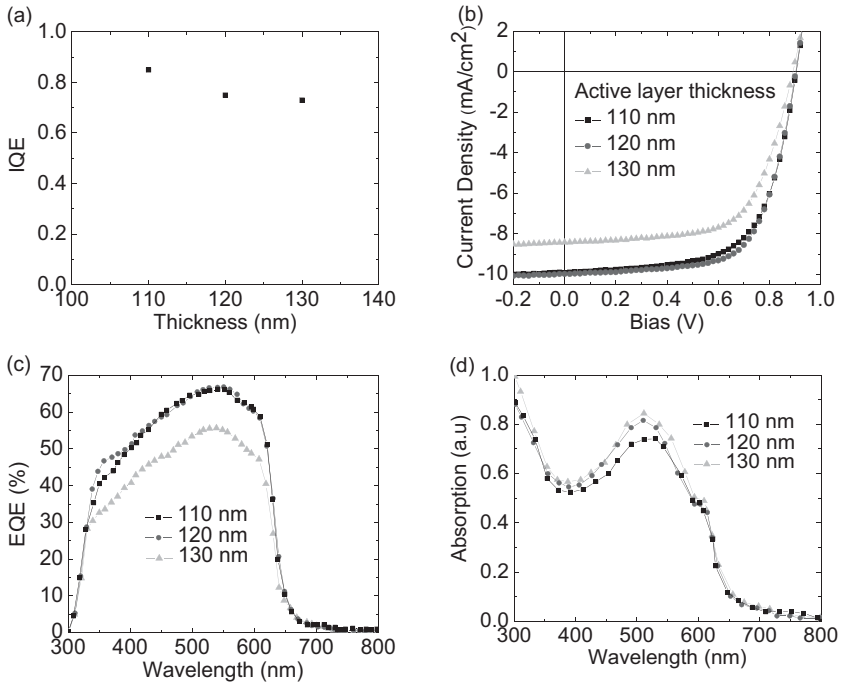


**Figure 2.** PSEHTT:$IC_{60}BA$-based single-junction solar-cell performance with different active layer thicknesses and different hole-transporting layers under simulated AM1.5G illumination. a) Internal quantum efficiency, b) J–V curves, c) external quantum efficiency, and d) absorption.

averaged IQEs is 76% for PSEHTT:$IC_{60}BA$ with a standard deviation of 3%. The peak IQE reached 80% for 220 nm thickness, and the IQE value slightly decreased with the increase of photoactive layer thickness. As the photoactive layer thickness increases, the charge recombination loss also increases. Thus, this approach does not guarantee a high-performing solar cell.

Figure 3b demonstrates the photo J–V characteristics of the single junction as a function of PSBTBT:$PC_{70}BM$ BHJ layer thickness under 100 mW/cm$^2$ AM1.5G illumination. As seen in **Table 2**, the $J_{sc}$ of the single-junction solar cells increases with increasing thickness of PSBTBT:$PC_{70}BM$ BHJ layer and its value increases from 13.24 mA/cm$^2$ for the cell with a 210 nm thickness BHJ layer to 13.36 mA/cm$^2$ for the 220 nm-thick BHJ layer cell. The increase in $J_{sc}$ with the increasing thickness of the BHJ layer is attributed to the increase in light absorption and exciton generation. Notably, the FF increases with increasing thickness of BHJ layer from 54.11% for the cell with a 200 nm-thick BHJ layer to 58.36% for 220 nm-thick heterojunction layer cell. On the other hand, the $V_{oc}$ of the PSBTBT:$PC_{70}BM$ is 0.64 V and is independent of the thickness of the PSBTBT:$PC_{70}BM$ BHJ layer. The overall PCE of the PSBTBT:$PC_{70}BM$ cell increases with increasing thickness of the PSBTBT:$PC_{70}BM$ BHJ layer from 4.59% for the cell with a 200 nm-thick BHJ layer to 4.99% for a 220 nm-thick heterojunction layer cell. However, device efficiency decreases with the increase of PSBTBT:$PC_{70}BM$ BHJ layer from 220 to 230 nm. In this case, the $J_{sc}$ and FF plummet to 13.18 mA/cm$^2$ and 50.75%, respectively.

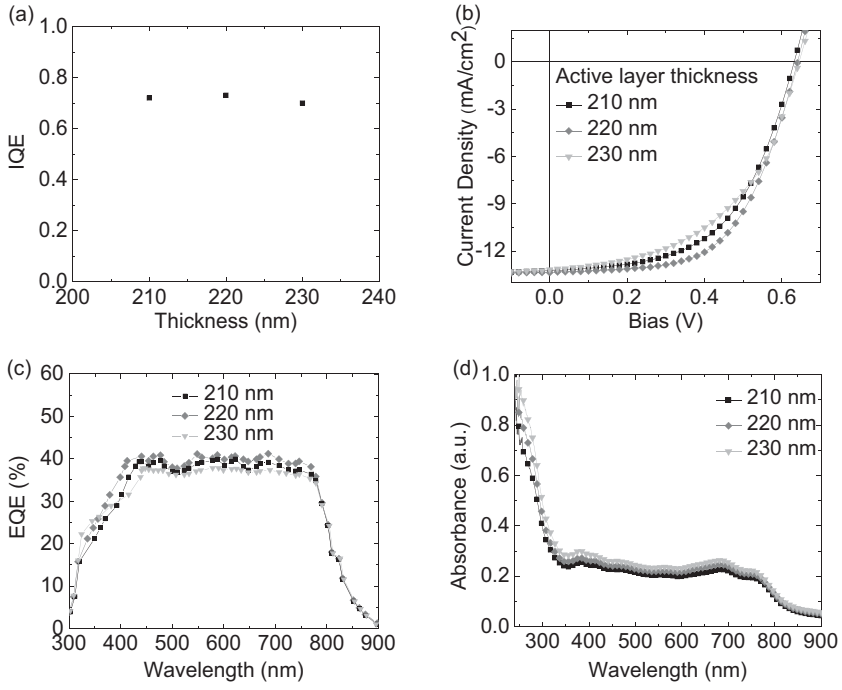


**Figure 3.** PSBTBT:$PC_{70}BM$-based single-junction solar-cell performance with different active layer thicknesses and different electron-transporting layers under simulated AM1.5G illumination. a) Internal quantum efficiency, b) J–V curves, c) external quantum efficiency, and d) absorption.

Figure 3c,d illustrate the EQE and the absorption plots of single junction, respectively. The PSBTBT:$PC_{70}BM$ cells have a strong EQE response in the infrared region with a peak response at about 740 nm with absorption extending to 900 nm. Furthermore, the photoresponse in the infrared regime rise with increasing PSBTBT:$PC_{70}BM$ BHJ layer thickness. The photoresponse spectra of the BHJ cells are consistent with the optical absorbance spectra for the PSBTBT:$PC_{70}BM$ mixed film. The maximum EQE value is about 62% at 740 nm wavelength in the single junction solar cells with a 220 nm thick PSBTBT:$PC_{70}BM$ BHJ layer, and the average is ~55%. The integrated EQEs for 210, 220, and 230 nm devices are 13.20, 13.31, and 13.12 mA/cm$^2$, respectively. These values are in agreement with the obtained $J_{sc}$ values from J–V characteristics. As shown in Figure 3d, absorption in infrared regions is as high as 85%; however, in visible regions, the average absorption is only 60%. Therefore, it is critical to enhance visible absorption, while preserving highly efficient charge transport and collection.

**Table 2.** Device performance of PSBTBT:$PC_{70}BM$-based inverted single junction solar cells with different BHJ layer thicknesses and different ETLs.

| Active layer thickness [nm] | ETL | $J_{sc}$ [mA/cm$^2$] | $V_{oc}$ [V] | FF [%] | PCE [%] |
|---|---|---|---|---|---|
| 210 | PEIE | 13.24 | 0.64 | 54.11 | 4.59 |
| 220 | PEIE | 13.36 | 0.64 | 58.36 | 4.99 |
| 230 | PEIE | 13.18 | 0.64 | 50.75 | 4.28 |
| 200 | GO | 13.19 | 0.64 | 54.23 | 4.58 |
| 200 | LZO | 12.85 | 0.64 | 36.82 | 3.03 |

**Table 3.** Device performance of front, rear, and tandem cells.

| Structure | $J_{sc}$ [mA/cm$^2$] | $V_{oc}$ [V] | FF [%] | PCE [%] |
|---|---|---|---|---|
| Front | 9.98 ± 0.7 | 0.91 ± 0.02 | 66.63 ± 1 | 5.99 ± 0.2 |
| Rear | 13.36 ± 0.4 | 0.64 ± 0.02 | 58.36 ± 0.02 | 4.99 ± 0.07 |
| Tandem | 8.73 ± 0.1 | 1.52 ± 0.02 | 67.15 ± 1 | 8.91 ± 0.05 |

Our observations from these two different independent evaluation experiments unveil strong and important correlations between charge recombination, ETL, HTL, and the film thickness. We conclude that 120 and 220 nm and PEDOT:PSS and PEIE are ideal BHJ thicknesses and an ETL and HTL that balance absorption, charge collecting, and charge transporting.

The device performance of the fully solution-processed inverted tandem cell (**Figure 4**, **Table 3**) demonstrates that the $V_{oc}$ of the tandem cell is 0.04 V less than the sum of the $V_{oc}$s of the front and rear subcells. Our most successful cell had $V_{oc}$ = 1.52 ± 0.02 V, $J_{sc}$ = 8.73 ± 0.1 mA/cm$^2$, FF = 67.15 ± 1%, and PCE = 8.91 ± 0.05%. The front subcell showed $V_{oc}$ = 0.91 ± 0.02 V, $J_{sc}$ = 9.98 ± 0.7 mA/cm$^2$, FF = 66.63 ± 1%, and PCE = 5.99 ± 0.2%. The control rear subcell showed $V_{oc}$ = 0.64 ± 0.02 V, $J_{sc}$ = 13.36 ± 0.4 mA/cm$^2$, FF = 58.36 ± 0.02%, and PCE = 4.99 ± 0.07%. Interestingly, the FF of the tandem cell was 67.15%, thus proving that the PEDOT:PSS/PEIE ICL is an excellent junction for both electrons and holes. Additionally, the high FF indicates that photogeneration in the tandem subcells is relatively field-independent. The improved FF is attributed to the redistribution of the built-in electric field in the subcells as a result of the required current matching in the subcells. The $J_{sc}$ of the tandem cell is lower than the front and rear subcells. This may be the result of the partial overlapped absorption of the PSEHTT:$IC_{60}BA$ and PSBTBT:$PC_{70}BM$ BHJ films at the visible region and the optical field redistribution in tandem structure when the two single-junction cells were stacked.

Figure 4b shows the EQE of each subcell within the tandem cell alongside the absorptance spectra of the corresponding photoactive layers in the device stacks. EQE measurements of the tandem solar-cell structures require special precaution due to coupled light-absorption and current-generation processes in each cell.[25] EQE measurements were performed with two excitation light sources, a 700 nm light optical bias light beam was used to excite only one of the subcells while a 550 nm light was used to measure the EQE of the other subcell. The EQE spectra demonstrate an excellent match in photocurrents generated by the front and rear subcells. The EQE spectra closely follow the absorptance spectra of the front and rear subcells, confirming that the photocurrents render from photoactive layers. Another important consideration in tandem cells is their stability. The single-junction solar cell is known to degrade 25–30% under continuous illumination, even when encapsulated.[26]

Figure 4c demonstrates efficiency versus storage time in air of the tandem cell without encapsulation. The tandem cell was fabricated using an ITO/ZnO/PSEHTT:$IC_{60}BA$/PEDOT:PSS/PEIE/PSBTBT:$PC_{70}$-BM/$MoO_3$/Ag structure. The PCE with an initial value of 8.91% remains at 8.61% after 720 h storage in air and remains above 90% of the original value even after storage in air for 60 days. As is well known,[21] inverted cells have much better stability in air compared to conventional cells. Despite this remarkable improvement in stability with the inverted structure, the degradation mechanism in solar cells remains unclear, and requires detailed studies to fully understand it and further improve the stability.

More than 138 tandem cells were made, with the best device demonstrating an 8.91%. In the course of these studies, we created more than 109 tandem cells with efficiencies greater than 8.5%.

Furthermore, in achieving high-performance tandem cells, the optimized BHJ layer thickness of the front and rear subcells is crucial for balanced optical absorptions and matched currents. Photocurrent in tandem cells is limited by the photocurrent of the front subcell, thus it is important to control FF for effi-

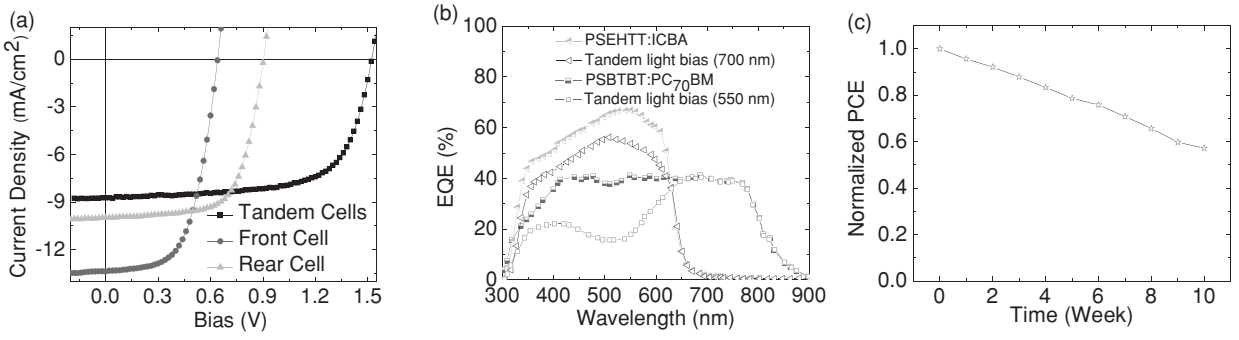


**Figure 4.** a) J–V curves of front, rear, and tandem cells. b) EQE measured under relevant bias illumination conditions. c) Stability of unencapsulated tandem cell over 10 weeks.

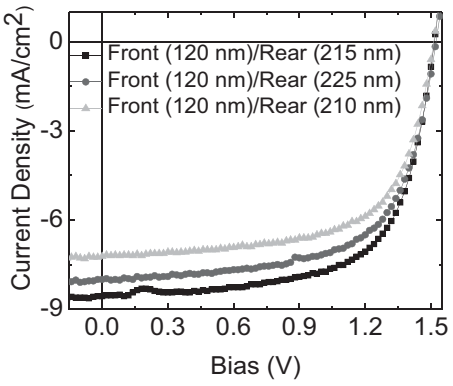


**Figure 5.** J–V curves of tandem cells with various thicknesses of rear subcell.

cient tandem cells. Current matching between subcells in series tandem cells is critical: the number of absorbed photons,[27] charge carrier transport, and bimolecular recombination[28] must be optimized to balance the photocurrents. Low carrier mobilities and unbalanced electron/hole mobilities in organic solar cells[29,30] are characteristic of organic solar cells, making it complicated to match current densities between subcells.

Hence, a series of tandem cells were carefully designed to scrutinize the effect of rear subcell thickness on the performance of devices. Particularly, the PSBTBT:$PC_{70}$BM BHJ layer thicknesses varied from 210 to 225 nm. We fixed our PSEHTT:$IC_{60}$BA BHJ thickness at 120 nm in order to match the current between the front and rear subcells and keep sufficient absorption and photocurrent in the rear subcell. **Figure 5** demonstrates resultant photo J–V plots of three different sets of tandem cells with different PSBTBT:$PC_{70}$BM BHJ thicknesses. Photovoltaic parameters obtained from J–V plots are listed in **Table 4**. We found that these three tandem cells provide $V_{oc}$ = 1.52 V. One could observe from Table 4 that the variation of the PSBTBT:$PC_{70}$BM BHJ layer thickness affected both $J_{sc}$ and FF for all tandem cells less compared to the ideal tandem having 120 and 220 nm for the front and rear subcells.

As we decrease the PSBTBT:$PC_{70}$BM BHJ thickness from 220 to 215 nm, our tandem cell still maintain its performance, in which there is a negligible drop in $J_{sc}$. However, there is a minor decrease in FF from 67.15 to 66.63% leading to 8.47% PCE. The drop in FF is due to the increase in $R_s$ from 12.3 to 15.6 Ω $cm^2$. However, if we increase the thickness of PSBTBT:$PC_{70}$BM BHJ layer, the tandem cell demonstrates a dramatic decrease in $J_{sc}$ as well as FF. In the case for 225 nm thick of PSBTBT:$PC_{70}$BM BHJ layer, the $J_{sc}$ = 8 mA/$cm^2$, FF = 64.14% along with 7.80% PCE.

Declining tandem cell performance can be observed in the case of 210 nm thick of PSBTBT:$PC_{70}$BM BHJ layer. In this cell, the $J_{sc}$ falls to its lowest value of 7.23 mA/$cm^2$ while FF drops to 63.19%. The overall PCE for 210 nm thick of PSBTBT:$PC_{70}$BM cell is 7.05%. As discussed above, the loss of $J_{sc}$ in the thinner rear subcell is due to lower dissociation rate of excitons, while the loss in thicker rear subcell is due to the slower drifting of charges which leads to recombination of separated charges.

Many interesting and new ICL concepts have been established in recent years.[3–11] In search for a new and ideal ICL, we assert that the ICL not only serves as the charge recombination electrode between those subcells, but ensures the presence of suitable interface energy for efficiently recombining the charges from the subcells. Furthermore, it must prevent any generation of a reverse built-in potential that might reduce the $V_{oc}$ of tandem cell. Thus, ICL must be optically transparent to avoid any absorption and reflection when projected light passes through the rear subcell into the front subcell. We extended our investigation on tandem cells using three different sets of ICLs including i) PEDOT:PSS/Zinc Oxide (ZnO), ii) neutral-PEDOT:PSS(n-PEDOT:PSS)/ZnO, and iii) Graphene (G)/Titanium Oxide ($TiO_x$). The detailed photovoltaic parameters of the corresponding tandem cells are tabulated in **Table 5**. As shown in this table, the cells performance varied remarkably with different ICLs. This indicates that the ICL plays a vital role in the charge recombination process. These observations also indicate that tandem cells with a ICL of PEDOT:PSS/ZnO, n-PEDOT:PSS/ZnO, and G/$TiO_x$ have smaller $V_{oc}$'s of 1.4, 1.2, and 1.12 V which are lower compared with PEDOT:PSS/PEIE ICL. We attributed the low $V_{oc}$'s to the energy barrier, causing a large voltage drop across these ICLs. In addition, lower FFs correspond to larger internal resistance and inefficient charge extraction and recombination at the ICLs. It is also worth noting that a solvent resistance study on PEDOT:PSS/PEIE ICL using various solvents has been conducted and the PEDOT:PSS/PEEIE demonstrated good chemical resistance from cholorobenze, 1,2-dicholorobenzene, and 1,3,5-tricholorobenzene.[31] This implies that PEDOT:PSS/PEIE can be considered a good and robust ICL to prevent any solvent penetration upon the deposition of the rear subcell.

Importantly, no S-shaped kink curve was observed in the positive bias regime. In the S-shaped kink curve, as bias voltage increases, the current just levels off and again increases in the vicinity of the $V_{oc}$ regime. This leads to the decrease in FF and PCE. This behavior has frequently been seen not only in degraded J–V characteristics but also in the J–V characteristics immediately after the fabrication of solar cells. Several

**Table 4.** Device performance of tandem cells with different rear subcell thicknesses.

| Active layer thickness (Front/Rear) [nm] | $J_{sc}$ [mA/$cm^2$] | $V_{oc}$ [V] | FF [%] | PCE [%] |
|---|---|---|---|---|
| 120/215 | 8.56 | 1.52 | 65.12 | 8.47 |
| 120/225 | 8.00 | 1.52 | 64.14 | 7.80 |
| 120/210 | 7.23 | 1.52 | 63.19 | 7.05 |

**Table 5.** Device performance of tandem cells with different ICLs.

| Interconnecting layer | $J_{sc}$ [mA/$cm^2$] | $V_{oc}$ [V] | FF [%] | PCE [%] |
|---|---|---|---|---|
| PEDOT:PSS/ZnO | 9.17 | 1.4 | 64.65 | 8.30 |
| n-PEDOT:PSS/ZnO | 8.05 | 1.2 | 62.52 | 6.04 |
| G/$TiO_x$ | 7.21 | 1.14 | 62.20 | 5.11 |

theoretical models have been put forward to explain the mechanism of the S-shaped kink curve.[32,33] Glatthaar et al. suggested that the origin of the S-shaped kink is from doping and corrosion of the top contact as well as a thin-current limiting layer under forward bias.[34] Wang et al. ascribed the presence of S-shaped kink curve to charge accumulation and interfacial recombination induced by the cathode buffer layer.[35] 5 Kumar et al. proposed that strong interface dipole, defects and traps are the responsible entities leading to the presence of S-shaped kink curve.[33] On the other hand, the S-shaped kink has been overcome by the appropriate selection of electrodes and buffer materials, surface treatments, and doping. Walzer et al. introduced a doping method in phthalocyanines on a transparent electrode to achieve high conductivity and to suppress the S-shaped kink.[36]

In previously published works where $MoO_3$/Al/ZnO,[21] Al/$TiO_2$/PEDOT:PSS,[37] and ZnO/PEDOT:PSS[38] were used as ICLs, the S-shaped kink curves were completely eliminated after surface treatment. In another case, Timmreck et al.[4] proposed using a highly doped layer in order to completely remove the S-shaped kink curve. Recently, Yang et al.[21] were able to remove the S-shaped kink curve from their tandem cell by manipulating the interface energy with the incorporation a good ohmic contact material. Although many reports on the S-shaped kink curve have been presented, the generation mechanism is not well understood. Detailed investigations on S-shaped kink in tandem cell are currently under progress and will be treated elsewhere.

## 3. Conclusion

We have fabricated high performance inverted tandem solar cells and investigated the effects of ICL as well as thickness matching on the device performance. Our results indicate that the formation of quasi-ohmic-contact in PEDOT:PSS/PEIE ICL provides an efficient recombination zone for holes and electrons generated from the front and rear subcells. Furthermore, optical transmission through the front subcell maximized the optical absorption of the rear subcell. The effectiveness of the optimized tandem cell reached a maximum PCE of 8.91% and the measured $V_{oc}$ was 1.52 V. This study suggests new avenues for creating universal device layouts and enhancing the efficiency of future inverted tandem cells. More effort must be directed towards large area fabrication and high productivity such as roll-to-roll production of inverted tandem cell.

## 4. Experimental Section

*Materials*: PSEHTT was synthesized according to previous publications and can be found elsewhere.[38] PEDOT:PSS, $IC_{60}BA$, PSBTBT, and $PC_{70}BM$, $MoO_3$, and PEIE were purchased from HC Starck, Lumtec, Solarmer, and Sigma Aldrich, respectively and used without further purification.

*Single Junction Fabrication (Front Subcell)*: The pre-cleaned ITO substrates were first treated with UV-ozone for 10 min. PEIE ($M_w$ = 70 000 g/mol) was dissolved in $H_2O$ with a concentration of 35–40 wt% when received from Aldrich. It was then further diluted with 2-methoxyethanol to a weight concentration of 0.4%. After, the solution was spin-coated on the ITO substrates at a spin speed of 5000 rpm for 1 min. The approximate thickness of the film is 10 nm. Spin-coated PEIE film was annealed at 100 °C for 10 min in ambient air. Then, the active layer was spin coated on the PEIE layer. Poly[(4,4′-bis(3-ethyl-hexyl) dithieno[3,2-b:″3′-d]silole)-2,6-diyl-alt-(2,5-(3-(2-ethyl-hexyl)thiophen-2-yl)thiazolo[5,4-d]thiazole]:indene-$C_{60}$ bisadduct (PSEHTT:$IC_{60}BA$) (1:1, weight ratio) was dissolved in a solvent mixture of 1,2-dichlorobenzene (ODCB) and 1,8-octanedithiol (ODT) (ODCB:ODT = 100:2.5, v/v) for the first active layer. After spin-coating the active layer, the samples are transferred into the evaporation chamber for fabricating the HTL and finally LiF:Al electrode, the device area is 0.04 $cm^2$.

*Single Junction Fabrication (Rear Subcell)*: The pre-cleaned ITO substrates were first treated with UV-ozone for 10 min. ETL was spin-coated on the ITO substrates. Then the active layer was spin-coated on the ETL layer. The rear subcell active layer was spin-coated at 4500 rpm for 1 min from PSBTBT:$PC_{70}BM$ (1:1) in chloroform (10 mg of PSBTBT/1 mL of solvent) and thermally annealed at 150 °C for 5 min. After spin-coating the active layer, the samples were transferred into the evaporation chamber for fabricating the $MoO_3$/Ag electrode, the device area is 0.04 $cm^2$.

*Tandem Devices Fabrication*: The front and rear subcells were made according to the single junction procedure. Samples were transferred into the glove-box for PEDOT:PSS layer deposition; the thickness of PEDOT:PSS is 40 nm. The PEIE was spin-casted on PEDOT:PSS layer, the details of modified PEDOT:PSS can be found elsewhere.[11] And then the rear subcell was fabricated as the front subcell; the thicknesses of the active layer were controlled by the spin coating speed. Finally, the samples were transferred into the evaporation chamber for fabricating the $MoO_3$ (10 nm)/Ag (100 nm) electrode; the device area is 0.04 $cm^2$.

*Device Characterization*: For tandem solar cells, the layers comprising PEIE/PSEHTT:$IC_{60}BA$/PEDOT:PSS/PEIE/PSBTBT:$PC_{70}BM$ were electrically isolated using toluene and methanol along the perimeter defined by the area of the top electrode. This isolation avoids fringing effects and also prevent over estimation of the photocurrents generated by the tandem cell. During the measurements and stability tests, a shadow mask (0.04 $cm^2$) with a single aperture was placed onto the tandem solar cells in order to define its photoactive area. The current density–voltage (*J–V*) characteristics were recorded with a Keithley 2410 source unit. The EQE measurements were performed using EQE system (Model 74000) obtained from Newport Oriel Instruments USA and HAMAMATSU calibrated silicon cell photodiode used as a reference diode. The wavelength was controlled with a monochromator 200–1600 nm.

## Acknowledgements

This work was supported by CAPES-PNPD Project No. 3076/2010 and Industrial Strategic Technology Development (10045269, Development of Soluble TFT and Pixel Formation Materials/Process Technologies for AMOLED TV) funded by MOTIE/KEIT. The authors also would like to thank First Solar Team for helping with stability test.

Received: October 9, 2013
Published online: December 19, 2013

[1] Z. He, C. Zhong, S. Su, M. Xu, H. Wu, Y. Cao, *Nat. Photon.* **2012**, *6*, 591.
[2] M. Hiramoto, M. Seuzaki, M. Yokoyama, *Chem. Lett.* **1990**, *19*, 327.
[3] M. Riede, C. Uhrich, J. Widmer, R. Timmrecck, D. Wynands, G. Schwartz, W. M. Gnehr, D. Hildebrandt, A. Weiss, J. Hwang, S. Sundarraj, P. Erk, M. Pfeiffer, K. Leo, *Adv. Funct. Mater.* **2011**, *21*, 3019.
[4] R. Timmreck, S. Olthof, K. Leo, M. K. Riede, *J. Appl. Phys.* **2010**, *108*, 033108.
[5] P. Peumans, A. Yakimov, S. R. Forrest, *J. Appl. Phys.* **2004**, *93*, 3693.

[6] A. Hadipour, B. de Boer, P. W. M. Blom, *Adv. Funct. Mater.* **2008**, *18*, 169.
[7] S. Sista, M. H. Park, Z. R. Hong, Y. Wu, J. H. Hou, W. L. Kwan, G. Li, Y. Yang, *Adv. Mater.* **2010**, *22*, 380.
[8] J. G. Xue, S. Uchida, B. P. Rand, S. R. Forrest, *Appl. Phys. Lett.* **2004**, *85*, 5757.
[9] X. W. Sun, D. W. Zhao, L. Ke, A. K. K. Kyaw, G. Q. Lo, D. L. Kwong, *Appl. Phys. Lett.* **2010**, *97*, 053303.
[10] J. Y. Kim, K. Lee, N. E. Coates, D. Moses, T. Q. Nguyen, M. Dante, A. J. Heeger, *Science* **2007**, *317*, 222.
[11] J. Gilot, M. M. Wienk, R. A. J. Janssen, *Adv. Mater.* **2010**, *22*, E67.
[12] B. A. Gregg, M. C. Hana, *J. Appl. Phys.* **2003**, *93*, 3605.
[13] V. Bhosle, J. T. Prater, F. Yang, D. Burk, S. R. Forrest, J. Narayan, *J. Appl. Phys.* **2007**, *102*, 023501.
[14] K. Schulze, B. Maennig, K. Leo, Y. Tomita, C. May, J. Huepkes, E. Brier, E. Reinold, P. Baeuerle, *Appl. Phys. Lett* **2007**, *91*, 073521.
[15] W. Gaynor, J.-Y. Lee, P. Peumans, *ACS Nano* **2010**, *4*, 30.
[16] www.heliatek.com/newscenter/latestnews/, accessed: January, 2013.
[17] J. You, C.-C. Chen, Z. Hong, K. Yoshimura, K. Ohya, R. Xu, S. Ye, J. Gao, G. Li, Y. Yang, *Adv. Mater.* **2013**, DOI: 10.1002/adma.201300964
[18] J. You, L. Dou, K. Yoshimura, T. Kato, K. Ohya, T. Moriarty, K. Emery, C.-C. Chen, J. Gao, G. Li, Y. Yang, *Nat. Commun.* **2012**, *4*, 1446.
[19] D. W. Zhao, L. Ke, Y. Li, S. T. Tan, A. K. K. Kyaw, H. V. Demir, X. W. Sun, D. L. Carroll, G. Q. Lo, D. L. Kwong, *Sol. Energy Mater. Sol. Cells* **2011**, *95*, 921.
[20] X. W. Sun, D. W. Zhao, L. Ke, A. K. K. Kyaw, G. Q. Lo, D. L. Kwong, *Appl. Phys. Lett.* **2010**, *97*, 053303.
[21] C.-H. Chou, W. L. Kwan, Z. Hong, L.-M. Chen, Y. Yang, *Adv. Mater.* **2011**, *23*, 1282.
[22] S. K. Hau, H.-L. Yip, K.-S. Chen, J. Zou, A. K.-Y. Jen, *Appl. Phys. Lett.* **2010**, *97*, 253307.
[23] A. R. B. M. Yusoff, W. J. da Silva, H. P. Kim, J. Jang, Nanoscale 2013, 5, 11051.
[24] L. J. A. Koster, E. C. P. Smits, V. D. Mihailetchi, P. W. M. Blom, *Phys. Rev. B* **2005**, *72*, 085205.
[25] J. Gilot, M. M. Wienk, R. A. J. Janssen, *Adv. Funct. Mater.* **2010**, *20*, 3904.
[26] C. H. Peters, I. T. S. Quitana, J. P. Kastrop, S. Beaupré, M. Leclerc, M. D. McGehee, *Adv. Energy Mater.* **2011**, *1*, 491.
[27] G. Dennler, K. Forberich, T. Ameri, C. Waldauf, P. Denk, C. J. Brabec, *J. Appl. Phys.* **2007**, *102*, 123109.
[28] A. Pivrikas, N. S. Sariciftci, G. Juska, R. Osterbacka, *Prog. Photovoltaics* **2007**, *15*, 677.
[29] M. Lenes, L. J. A. Koster, V. D. Mihailetchi, P. W. M. Blom, *Appl. Phys. Lett.* **2006**, *88*, 243502.
[30] L. J. A. Koster, V. D. Mihailetchi, P. W. M. Blom, *Appl. Phys. Lett.* **2006**, *88*, 052104.
[31] A. Wagenpfahl, D. Rauh, M. Binder, C. Deibel, V. Dyakonov, *Phys. Rev. B* **2010**, *82*, 115306.
[32] A. Kumar, S. Sista, Y. Yang, *J. Appl. Phys.* **2009**, *105*, 094512.
[33] M. Glatthaar, M. Riede, N. Keegan, K. Sylvester-Hvid, B. Zimmermann, M. Niggermann, A. Hinsch, A. Gombert, *Sol. Energy Mater. Sol. Cells* **2007**, *91*, 390.
[34] J. C. Wang, X. C. Ren, S. Q. Shi, C. W. Leung, P. K. L. Chan, *Org. Electron.* **2011**, *12*, 880.
[35] K. Walzer, B. Maening, M. Pfeiffer, K. Leo, *Chem. Rev.* **2007**, *107*, 1233.
[36] S. Sista, M.-H. Park, Z. Hong, Y. Wu, J. Hou, W. L. Kwan, G. Li, Y. Yang, *Adv. Mater* **2010**, *22*, 380.
[37] J. Gilot, M. M. Wienk, R. A. J. Janssen, *Appl. Phys. Lett.* **2007**, *90*, 143512.
[38] H. Xin, S. Subramaniyan, T.-W. Kwon, S. Shoaee, J. R. Durrant, S. A. Jenekhe, *Chem. Mater.* **2012**, *24*, 1995.